JOURNAL OF GUIDANCE, CONTROL, AND DYNAMICS
Vol. 31, No. 6, November–December 2008

Simultaneous Realization of Handling and Gust Responses: In-Flight Simulator Controller Design

Masayuki Sato*
Japan Aerospace Exploration Agency, Tokyo 181-0015, Japan
and
Atsushi Satoh†
Iwate University, Iwate 020-8551, Japan

DOI: 10.2514/1.36713

This paper addresses the design problem of a flight controller for an in-flight simulator, in which the controller is required to realize the gust response and the handling response of the target aircraft simultaneously. A two-degree-of-freedom model-matching controller is proposed to meet this requirement, with feedback and feedforward controllers designed to vary the gust response and handling response characteristics, respectively. The controller is designed in two steps: the feedback controller is first designed via the H_∞ model-matching approach, then the feedforward controller is designed as a filtered right inverse system of the closed-loop system comprising the plant dynamics and the feedback controller. Controllers are designed to enable a research aircraft to simulate the lateral–directional motions of two target aircraft models: a Boeing 747 and a Convair 880M. Hardware-in-the-loop simulations and flight tests with the designed controllers confirm that they achieve the simultaneous realization of gust response and handling response of the target aircraft. Additionally, an in-flight simulator controller for investigating handling qualities for lateral–directional motions is designed, and hardware-in-the-loop simulations and flight tests confirm its applicability to handling-quality investigation.

Nomenclature

F	=	feedforward controller
$G(s)$	=	transfer function of system G
$\|G(s)\|_\infty$	=	H_∞ norm of system G
I_n	=	n-dimensional identity matrix
K	=	feedback controller
$M_{z_m u_m}$	=	dynamics of target aircraft from handling input to output
$M_{z_m w_g}$	=	dynamics of target aircraft from wind gust to output
P	=	dynamics of plant
P_n	=	nominal dynamics of P
$\mathcal{R}^{n\times m}$	=	set of $n \times m$-dimensional real matrices
r	=	yaw rate
$\mathcal{S}^n$	=	set of $n \times n$-dimensional real symmetric matrices
u_m	=	target aircraft handling input
u_{fb}	=	feedback control input
u_{ff}	=	feedforward control input
u_p	=	plant control input
v_a	=	lateral air velocity
v_g	=	lateral gust velocity
v_i	=	lateral inertial velocity
w_g	=	wind gust input
$\|X\|$	=	maximum singular value of matrix X
$\langle X \rangle$	=	$X + X^T$
y	=	plant measurement output
z_m	=	target aircraft output
z_p	=	plant controlled output
δ_a, δ_{a_c}	=	aileron deflection and command
δ_r, δ_{r_c}	=	rudder deflection and command
$\mu_\Delta(X)$	=	structured singular value of matrix X with structured uncertainty Δ
p	=	roll rate
ϕ	=	roll angle
ψ	=	yaw angle
$\mathbf{I}$	=	appropriately dimensioned identity matrix
$\mathbf{0}$	=	appropriately dimensioned zero matrix
0_n	=	n-dimensional square zero matrix

I. Introduction

IN-FLIGHT simulators (IFSs) are useful tools for investigating flying qualities, handling qualities, aircraft development, and other applications [1], and much research into developing IFSs has been conducted since the 1970s (e.g., [1–5]). As pointed out in [1], the most important requirement for an IFS flight controller is to realize real-world cues; that is, the controller must realize the responses of the target aircraft.‡ An aircraft's motions are affected by the pilot's handling inputs and by wind gusts and so they comprise two components: a handling response (HR) and a gust response (GR). An IFS flight controller should therefore realize both of these target aircraft responses, but to the authors' knowledge, existing design methods realize only one of these two responses: model-following controllers [2,3,6] realize the HR of the target aircraft but do not consider GR realization; model-matching or loop-shaping-based designs [5,7–12] can realize the HR of the target aircraft but hardly consider GR realization; and although eigenstructure-assignment-based design [13–15] can realize the GR of the target aircraft by assigning the eigenstructure of the original aircraft to be close to that of the target, it cannot fully realize the HR without adding prefilters (i.e., feedforward controllers). Although the realization of HR is very important for IFSs, GR realization is essential for some applications: for example, evaluation of flying qualities or handling qualities during approach and landing. Because wind gusts are inevitably encountered during flight tests, a controller that can realize both types of responses simultaneously has been

Received 17 January 2008; revision received 24 March 2008; accepted for publication 24 March 2008.

*Researcher, Institute of Space Technology and Aeronautics, 6-13-1 Osawa, Mitaka; sato.masayuki@jaxa.jp.

†Associate Professor, Department of Mechanical Engineering, 4-3-5 Ueda, Morioka; satsushi@iwate-u.ac.jp.

‡In this paper, the aircraft for which the response is to be realized is referred to as the *target aircraft* and the aircraft in which an IFS system is implemented is referred to as the *original aircraft*.

desired for IFSs. Realizing both HR and GR using model-following controllers or reference-tracking controllers, which are widely used for tracking problems, may be possible with the following approach. A feedback controller is first designed to alleviate the GR of the original aircraft, and a model-following controller or a reference-tracking controller is then designed for the augmented system comprising the original aircraft dynamics and the feedback controller to realize the combined response of the target aircraft driven by gust and handling inputs. However, with this approach, it is generally impossible to totally eliminate the response of the original aircraft to gusts; moreover, online gust estimation, one of the effective methods for which has successfully been demonstrated in [16], is required with the accompanying increase of controller complexity. Considering these issues, IFS flight controllers, which need neither GR alleviation nor online gust estimation, are desirable.

This paper proposes a new design framework for IFS controller design for the simultaneous realization of the GR and the HR of a target aircraft. The proposed controller is a two-degree-of-freedom model-matching controller (see Fig. 1) in which the feedback controller is designed for GR realization and the feedforward controller is designed only for HR realization. The design requirements for the two-degree-of-freedom controller (i.e., a pair of F and K in Fig. 1) are as follows:

GR realization: Under $u_m = \mathbf{0}$ (consequently, $u_{\mathrm{ff}} = \mathbf{0}$), the response from w_g to z_p of the original aircraft is made to be as close as possible to that of the target aircraft (i.e., $M_{z_m w_g} w_g$) by designing K appropriately.

HR realization: Under $w_g = \mathbf{0}$, the response from u_m to z_p is made to be as close as possible to that of the target aircraft (i.e., $M_{z_m u_m} u_m$) for any u_m by designing F and K appropriately.

If these requirements are satisfied, then the original aircraft controlled with F and K will simultaneously realize the GR and HR of the target aircraft; that is, the controlled original aircraft will move like the target aircraft in response to pilot handling inputs and wind gusts.

Designing F and K simultaneously via the H_∞ model-matching approach may be possible, but much tuning will be needed to find the best pair of F and K, because two completely different requirements are imposed; moreover, the increase of the fictitious uncertainty block associated with controller performance in H_∞ design generally leads to conservatism and, consequently, poor model-matching performance. To avoid such problems we use a two-step design approach: First, under the assumption that $u_m = \mathbf{0}$, the feedback controller K is designed for GR realization via the H_∞ model-matching approach. Second, under the assumption that $w_g = \mathbf{0}$, the feedforward controller F is designed for HR realization as a right inverse system of the closed-loop system comprising the dynamics of the original aircraft and the feedback controller K.

Considering that $M_{z_m u_m}$ generally has very low gains at high frequencies and that u_m is applied by a human pilot, the right inverse system is required to have right inverse performance only at low and middle frequencies; that is, F is merely to be a filtered right inverse system. However, designing a stable inverse system is more difficult if the closed-loop system potentially has unstable zeros, as shown in [17] and references therein, which is the case with our design. To accommodate this difficulty, the method in [5] is used to design the filtered right inverse system because it is applicable to systems with unstable zeros and its applicability to flight controller design has been demonstrated.

For the feedback controller, a controller that is robust against plant uncertainties is designed. However, plant uncertainties are not considered in the design of the feedforward controller because robust

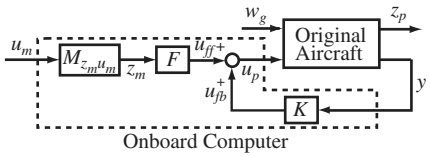

Fig. 1 Controller block diagram.

Fig. 2 Research aircraft MuPAL-α.

feedforward controller design is generally difficult, as feedforward controllers cannot reduce the effects of uncertainties. The robust performance of the feedforward controller against plant uncertainties is therefore confirmed a posteriori via μ analysis. As with feedback controller design, the feedforward controller can be designed via the model-matching technique shown in [8]. However, in general, the cascaded system comprising the filtered right inverse system and $M_{z_m u_m}$ is easier to implement within the limited resources of an onboard flight control computer than with a model-matching feedforward controller designed via the H_∞ model-matching approach, as noted in [5]. Therefore, in this paper, the feedforward part is composed of the filtered right inverse system F and the dynamics of the target aircraft HR model $M_{z_m u_m}$.

Using the proposed method, IFS controllers for the linearized lateral–directional (L/D) motions of Boeing 747 (B747) and Convair 880M (C880M) target aircraft are designed for the Japanese Aerospace Exploration Agency's multipurpose aviation laboratory (MuPAL-α) research aircraft (Fig. 2). Hardware-in-the-loop (HIL) simulations and flight tests confirm that the simultaneous realization of HR and GR of both target aircraft is fully achieved. In addition, an IFS controller for the investigation of L/D motion handling qualities is designed, and HIL simulations and flight tests confirm that the designed controller can be used for handling-quality investigations. The contribution of this paper is the proposal of a new design framework with a practical design technique for IFS controllers that achieve simultaneous realization of GR as well as HR and the demonstration of its applicability by experiments.

This paper is organized as follows: Sec. II describes briefly the controller design framework, Sec. III details the design of two IFS controllers for real target aircraft models and shows experimental results, Sec. IV describes the design of an IFS controller for handling-quality investigation and shows experimental results, and Sec. V gives concluding remarks.

II. Controller Design Framework

A. Feedback Controller Design

To achieve GR realization, the H_∞ model-matching technique, which has been widely reported (for example, [7,9]), is used in this paper. Hereafter, $\mathtt{diag}(X_1, \ldots, X_k)$ and $\mathtt{diag}_{1,k}(X_i)$ both denote the diagonal matrix composed of $X_1, \ldots, X_k$.

Suppose that plant uncertainties are modeled in the frequency domain, the time domain, or both and that their state-space models are given. Consequently, the plant dynamics incorporating the uncertainties is also supposed to be given. With a given plant dynamics, an appropriately defined stable diagonal weighting function W_1, which defines the model-matching performance of controller K, and a stable target aircraft model $M_{z_m w_g}$, the generalized plant P_g for designing controller K is given in Eq. (1) with the normalized uncertainty block:

$$\tilde{\Delta}_K := \mathtt{diag}(\Delta_u, \Delta_{p_K}) \qquad \| \tilde{\Delta}_K \| \leq 1$$

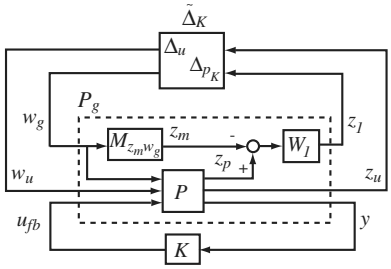

Fig. 3 Block diagram for feedback controller *K*.

where Δ_u and Δ_{p_K}, respectively, denote an uncertainty block with respect to the plant uncertainties and a fictitious performance block (see Fig. 3):

$$P_g: \begin{cases} \dot{x}_g = A_g x_g + B_{g1} w + B_{g2} u_{\text{fb}} \\ z = C_{g1} x_g + D_{g11} w + D_{g12} u_{\text{fb}} \\ y = C_{g2} x_g + D_{g21} w \end{cases} \tag{1}$$

where x_g is the state with $x_g = \mathbf{0}$ at $t = 0$, $w = [w_u^T \; w_g^T]^T$ is the disturbance input comprising the uncertain block output w_u and the wind gust input w_g, u_{fb} is the feedback control input, $z = [z_u^T \; z_1^T]^T$ is the controlled output comprising the uncertain block input z_u and the weighted performance output for model-matching performance, and y is the measurement output. The matrices A_g, etc., are constant matrices of appropriate dimensions.

If a feedback controller (which stabilizes the generalized plant and satisfies the inequality

$$\sup_{\omega \in \mathcal{R}} \mu_{\tilde{\Delta}_K}(G_{zw}(j\omega)) < 1 \tag{2}$$

where G_{zw} denotes the closed-loop system from w to z) is designed with a W_1 in which all the entries have sufficiently large gains in some frequency range, then the dynamics of the controlled plant from w_g to z_p become close to that of $M_{z_m w_g}$ in the frequency range under the prescribed plant uncertainties; that is, z_p becomes close to z_m for any w_g in the frequency range. Thus, the design problem for GR realization is given as follows:

Problem 1: Find controller K that stabilizes P_g and satisfies Eq. (2).

Further details on the design of K are given in Secs. III and IV with design examples.

B. Feedforward Controller Design

To achieve HR realization, feedforward controller F is designed as a filtered right inverse system of the closed-loop system comprising the plant dynamics and the previously designed K. The plant uncertainties are not considered when designing the feedforward controller, but its robust performance against uncertainties is checked a posteriori. If the performance is not satisfactory, the feedforward controller should be redesigned.

The block diagram for designing F is shown in Fig. 4, where P_n denotes the nominal dynamics of plant with gust input eliminated; K_{opt} is the feedback controller designed in the previous subsection; W_2 is a stable diagonal weighting function specifying the right inverse performance and frequency range of F; and w_2 and z_2 are, respectively, a fictitious disturbance input and a fictitious controlled output to define a filtered right inverse system. With an appropriately defined W_2, the design problem is to obtain a stable controller F that satisfies $\|G_{z_2 w_2}(s)\|_\infty < 1$, where $G_{z_2 w_2}$ denotes the system from w_2 to z_2. If the controller F is set to be full-order, which is the case with our design, then this is a standard H_∞ problem and so the details are omitted.

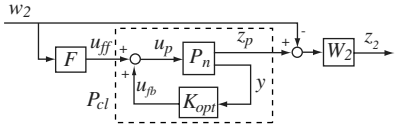

Fig. 4 Block diagram for feedforward controller *F*.

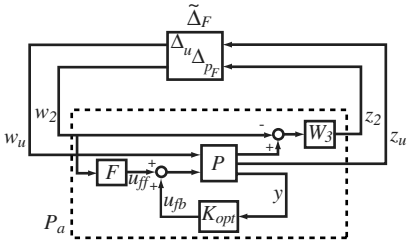

Fig. 5 Block diagram for the analysis of feedforward controller *F*.

If the feedforward controller F, which is stable, satisfies $\|G_{z_2 w_2}(s)\|_\infty < 1$, then the following Lemma holds for the cascaded system $P_o := P_{\text{cl}} F$, where P_{cl} denotes the closed-loop system comprising P_n and K_{opt} [5].

Lemma 1: Let $\zeta(\omega)$ be the minimum gain of W_2 at frequency ω; that is, $\zeta(\omega) := \min_i |W_i(j\omega)|$, and assume $\zeta(\omega) > 1$. Then the cascaded system P_o satisfies the following inequalities:

$$|P_{o_{ll}}(j\omega) - 1| < 1/\zeta(\omega) \quad \forall \; l \tag{3}$$

$$|\angle P_{o_{ll}}(j\omega)| < \arcsin 1/\zeta(\omega) \quad \forall \; l \tag{4}$$

$$|P_{o_{lm}}(j\omega)| < 1/\zeta(\omega) \quad \forall \; l, m \qquad l \neq m \tag{5}$$

where $P_{o_{lm}}(j\omega)$ denotes the (l, m) entry of $P_o(j\omega)$.

This Lemma, roughly speaking, indicates that if the minimum gain of W_2 is sufficiently large over some frequency range $\omega \in [\omega_l, \omega_h]$, then

$$P_o(j\omega) \approx \mathbf{I} \quad \forall\, \omega \in [\omega_l, \omega_h]$$

that is, the transfer function of P_o with designed controller F is approximately described as an identity matrix over the frequency range.

After designing F, its robust performance against the plant uncertainties, which have the same description as in the previous subsection, is checked via μ analysis. The block diagram for the analysis is shown in Fig. 5, where P is the same plant model as the P used in the feedback controller design but with the gust input eliminated; W_3 is the weighting function to define the right inverse performance and the frequency range of F (i.e., W_3 corresponds to W_2 in Fig. 4); and Δ_{p_F} and Δ_u are, respectively, the fictitious performance block and the uncertainty block with respect to the plant uncertainties.

If the upper μ for the augmented system P_a shown in Fig. 5 with the uncertainty block $\tilde{\Delta}_F := \texttt{diag}(\Delta_u, \Delta_{p_F})$ is less than unity for all frequencies, then the feedforward controller F is confirmed to satisfy Eqs. (3–5), in which W_2 is replaced by W_3, under the plant uncertainties; that is, F is confirmed to be a robust filtered right inverse system of the closed-loop system comprising the uncertain plant and the feedback controller. Further details of the design and analysis of F are given in Secs. III and IV with design examples.

III. IFS Controllers for the B747 and C880M Models

Using the design framework presented in the previous section, IFS controllers for two target aircraft models are designed: a B747 model flying at an altitude of 0 m and a true airspeed (TAS) of 67.4 [m/s], and a C880M model flying at an altitude of 0 m and a true airspeed of 68.9 m/s.

A. Controller Design

1. Plant and Model Descriptions

The plant model consists of the fourth-order linearized L/D motions of MuPAL-α at an equilibrium point, true airspeed TAS = 66.5 m/s, and altitude $H = 1520$ m. The state variables are

$$[v_i\,(\mathrm{m/s})\ p\,(\mathrm{rad/s})\ \phi\,(\mathrm{rad})\ r\,(\mathrm{rad/s})]^T$$

the gust input is v_g (m/s), the control inputs are $[\delta_a\,(\mathrm{rad})\ \delta_r\,(\mathrm{rad})]^T$, the controlled outputs are $[v_a\,(\mathrm{m/s})\ \phi\,(\mathrm{deg})]^T$, and the measurement outputs are

$$[v_a\,(\mathrm{m/s})\ p\,(\mathrm{rad/s})\ \phi\,(\mathrm{rad})\ r\,(\mathrm{rad/s})]^T$$

The MuPAL-α control actuators (i.e., aileron and rudder surfaces) are modeled as follows:

$$P_a\colon \begin{cases} \delta_a = \frac{0.72}{0.19s+1}\delta_{a_c} \\ \delta_r = \frac{0.77}{0.07s+1}\delta_{r_c} \end{cases} \tag{6}$$

The linearized L/D motions of MuPAL-α faithfully represent the L/D motions around the equilibrium point. However, there are uncertain delays between control surface command and control surface movement (i.e., dead time), and so delays with bounded delay time are added at the inputs of the actuator models. The delays are modeled using a first-order Padé approximation:

$$\frac{-T_i s/2+1}{T_i s/2+1}, \qquad T_i \in [T_{i_{\min}}, T_{i_{\max}}] \quad (i=1,2)$$

where index i denotes the number of inputs. This model can be represented as linear fractional transformation $\mathrm{LFT}(\Delta_d, P_d)$ with the following Δ_d and P_d (see Fig. 6):

$$\Delta_d := \mathtt{diag}(\delta_1, \delta_2) \qquad |\delta_i| \le 1 \qquad (i=1,2)$$
$$P_d\colon \begin{cases} \dot{x}_d = A_d x_d + B_{d_1} w_d + B_{d_2} u_p \\ z_d = C_{d_1} x_d + D_{d_{11}} w_d + D_{d_{12}} u_p \\ [\,\delta_{a_c} \quad \delta_{r_c}\,]^T = C_{d_2} x_d + D_{d_{21}} w_d + D_{d_{22}} u_p \end{cases} \tag{7}$$

where x_d denotes the state with $x_d = \mathbf{0}$ at $t=0$, z_d and w_d are both exogenous signals to define the delay model, and the state-space matrices of P_d are defined as follows:

$$\begin{bmatrix} A_d & B_{d_1} & B_{d_2} \\ C_{d_1} & D_{d_{11}} & D_{d_{12}} \\ C_{d_2} & D_{d_{21}} & D_{d_{22}} \end{bmatrix} = \begin{bmatrix} \mathtt{diag}_{1,2}(-(1/T_{i_{\min}} + 1/T_{i_{\max}})) & I_2 & \mathtt{diag}_{1,2}(2(1/T_{i_{\min}} + 1/T_{i_{\max}})) \\ \mathtt{diag}_{1,2}(-(1/T_{i_{\min}} - 1/T_{i_{\max}})) & 0_2 & \mathtt{diag}_{1,2}(2(1/T_{i_{\min}} - 1/T_{i_{\max}})) \\ I_2 & 0_2 & -I_2 \end{bmatrix}$$

The values of $T_{i_{\min}}$ and $T_{i_{\max}}$, respectively, are set to 0.08 and 0.16 for both aileron and rudder. These values are determined by summing the dead time for step commands with several amplitudes (0.04–0.12 s), the calculation time of the onboard flight control computers (0.02 s), and the time constants of the noise-reduction filters for measurement outputs (0.02 s). The nominal delays for aileron and rudder are both set to 0.12 s.

Then the plant P in Fig. 3 is given as shown in Fig. 6, in which the block denoted by L/D represents the linearized L/D motion model of MuPAL-α; $w_g \in \mathcal{R}$ represents gust input (i.e., v_g); and $w_d \in \mathcal{R}^2$ and $z_d \in \mathcal{R}^2$, respectively, correspond to w_u and z_u in Fig. 3. The state-space matrices of plant P are given in the Appendix as Eq. (A1).

The state-space matrices of the target models are calculated from [18]. The state variables, input variables, and output variables of the models are the same as those of the linearized L/D motion model of MuPAL-α. The actuators of the target aircraft are neglected in our design because their precise models are not given in [18]; however, they could be easily incorporated into our design if available. The state-space matrices $M_{z_m w_g}$ and $M_{z_m u_m}$ are shown in the Appendix.

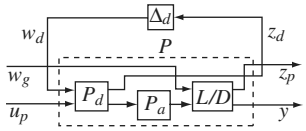

Fig. 6 L/D motion model with actuator model and uncertain delays.

2. Feedback Controller

One fictitious input is added to w_g to make Δ_{p_K} square. Then the uncertainty block $\tilde{\Delta}_K$ is composed of two real scalar blocks and one 2×2 complex full block. The weighting function for model-matching performance W_1 in Fig. 3 is set as follows:

$$W_1\colon \begin{cases} \gamma \frac{2s^2+s+1.1}{s^2+5.3s+1.1}\mathtt{diag}(1, 0.81) \\ \gamma \frac{2s^2+s+2.2}{s^2+3.9s+2.2}\mathtt{diag}(1, 0.67) \end{cases} \tag{8}$$

where the former weighting function is for the B747 model and the latter one is for the C880M model, and $\gamma(>0)$ is a design parameter to be maximized because the larger γ, the better the model-matching performance. These weighting functions have their lowest gains at the Dutch-roll mode frequency of the corresponding target aircraft. Unless the weighting function gains at the target aircraft's Dutch-roll mode frequency are lower than the gains at other frequencies, then the designed controller will have good model-matching performance only at the target aircraft's Dutch-roll mode frequency. The constant diagonal coefficient matrix in Eq. (8) is determined by considering the peak gains of v_a and ϕ of the target aircraft.

Because of the memory limitations of MuPAL-α's flight control computers, static output feedback controllers are designed. However, note that our design framework is directly applicable to dynamic controller design, which is worth considering for better performance if more computing resources are available.

After obtaining P_g in Eq. (1) from P, W_1, and $M_{z_m w_g}$, if γ is given, then problem 1 for the static output feedback controller using a constant scaling matrix S with respect to $\tilde{\Delta}_K$ is reformulated as follows:

Lemma 2: For a given $\gamma > 0$, if there exist symmetric matrices $P \in \mathcal{S}^{14}$ and S and controller K such that Eqs. (9–11) hold, then $\sup_{\omega\in\mathcal{R}} \mu_{\tilde{\Delta}_K}(G_{zw}(j\omega)) < 1$ holds:

$$P > 0 \tag{9}$$

$$S = \mathtt{diag}(s_1, s_2, s_3 I_2) > 0 \tag{10}$$

$$\begin{bmatrix} \langle PA_{\mathrm{cl}} \rangle & PB_{\mathrm{cl}} \\ B_{\mathrm{cl}}^T P & -S \end{bmatrix} + \begin{bmatrix} C_{\mathrm{cl}}^T \\ D_{\mathrm{cl}}^T \end{bmatrix} S [\,C_{\mathrm{cl}} \quad D_{\mathrm{cl}}\,] < 0 \tag{11}$$

where A_{cl}, B_{cl}, C_{cl}, and D_{cl} are the state-space matrices of the closed-loop system comprising P_g and K.

After applying the elimination Lemma [19] or the projection Lemma [20] to Lemma 2, our design problem is equivalently transformed to the following problem:

Problem 2:

$$\max_{P \in \mathcal{S}^{14}, X \in \mathcal{S}^{14}, S = \mathtt{diag}(s_1, s_2, s_3 I_2)} \gamma \quad \text{subject to} \quad \begin{bmatrix} P & \mathbf{I} \\ \mathbf{I} & X \end{bmatrix} > 0 \tag{12a}$$

$$\operatorname{rank} \begin{bmatrix} P & \mathbf{I} \\ \mathbf{I} & X \end{bmatrix} = 14 \tag{12b}$$

$$\begin{bmatrix} B_{g_2} \\ \mathbf{0} \\ D_{g_{12}} \end{bmatrix}^{\perp} \begin{bmatrix} \langle A_g X \rangle & B_{g_1} & X C_{g_1}^T \\ B_{g_1}^T & -S & D_{g_{11}}^T \\ C_{g_1} X & D_{g_{11}} & -S^{-1} \end{bmatrix} \begin{bmatrix} B_{g_2} \\ \mathbf{0} \\ D_{g_{12}} \end{bmatrix}^{\perp T} < 0 \tag{13}$$

$$\begin{bmatrix} C_{g_2}^T \\ D_{g_{21}}^T \\ \mathbf{0} \end{bmatrix}^{\perp} \begin{bmatrix} \langle P A_g \rangle & P B_{g_1} & C_{g_1}^T \\ B_{g_1}^T P & -S & D_{g_{11}}^T \\ C_{g_1} & D_{g_{11}} & -S^{-1} \end{bmatrix} \begin{bmatrix} C_{g_2}^T \\ D_{g_{21}}^T \\ \mathbf{0} \end{bmatrix}^{\perp T} < 0 \tag{14}$$

$$s_1 > 0, \qquad s_2 > 0, \qquad s_3 > 0 \tag{15}$$

where matrices A_g, B_{g_1}, etc., denote the state-space matrices of P_g.

Using the linearization algorithm in [21] to tackle the rank constraint (12b), the following iterative algorithm is obtained, which uses a bisection search for maximizing γ. Index i denotes the iteration number of the controller design step.

Algorithm 1:

1) Set $i = 0$ and scaling matrix $S = I_4$. Maximize γ subject to Eqs. (12–14), where P and X are decision variables. Obtain the corresponding controller K by solving Eq. (11) using the obtained P, where only the controller matrix K is a decision variable. Set $\gamma_i = \gamma$ and $K_i = K$.

2) Using K_i, maximize γ subject to Eqs. (9–11), where P and S are decision variables. Set $\hat{\gamma}_i = \gamma$.

3) Increment the iteration number: $i = i + 1$. Using the scaling matrix S obtained at the preceding step, maximize γ subject to Eqs. (12–14), where P and X are decision variables. Obtain the corresponding controller K by solving Eq. (11) using the obtained P, where only the controller matrix K is a decision variable. Set $\gamma_i = \gamma$ and $K_i = K$.

4) Using K_i, maximize γ subject to Eqs. (9–11), where P and S are decision variables. Set $\hat{\gamma}_i = \gamma$. If $\hat{\gamma}_i - \hat{\gamma}_{i-1} < \varepsilon$ holds, where ε is set as 1.0×10^{-4}, then stop iteration. Otherwise, return to step 3.

Remark 1: If step 1 cannot proceed, that is, if matrices P and X cannot be found with sufficiently small γ, then stabilizing static output controllers may not exist. In such a case, the degree of the controllers is to be increased.

This algorithm is similar to D-K iteration in μ synthesis [9,22] but does not use dynamic scaling matrices to reduce the computational complexity of designing K. The calculation of the LMIs was carried out using SeDuMi version 1.05 software [23] along with the YALMIP version 3 parser [24].

Maximum γ values of 1.7698 (B747 model) and 1.4273 (C880M model) are obtained. The corresponding optimal controller K_{opt} and the scaling matrix S are, respectively, shown in Eqs. (16) and (17):

$$K_{\text{opt}}: \begin{cases} \begin{bmatrix} 6.3040 \times 10^{-3} & 0.23147 & 0.10042 & 0.81281 \\ 9.3628 \times 10^{-4} & -0.31419 & 0.94285 & 2.4858 \end{bmatrix} \\ \begin{bmatrix} 0.016274 & 0.537941 & 0.24957 & 0.92461 \\ -3.6195 \times 10^{-3} & 0.099165 & 1.7458 & 3.5892 \end{bmatrix} \end{cases} \tag{16}$$

$$S: \begin{cases} \mathtt{diag}(0.10534, 0.029202, 6.5821 \times 10^{-4} I_2) \\ \mathtt{diag}(0.022297, 8.1526 \times 10^{-3}, 9.4684 \times 10^{-4} I_2) \end{cases} \tag{17}$$

where the former matrices are for the B747 model and the latter ones are for the C880M model.

Figures 7 and 8 show the Bode plots of the closed-loop system with IFS controllers, respectively, for the B747 and C880M models, the uncontrolled plant, and the target aircraft from v_g to v_a and ϕ. Although they mostly overlap, four lines for the closed-loop system are drawn showing the combinations of maximum and minimum delay times for aileron and rudder inputs. The figures confirm that although the dynamics of the target models to wind gust are much different from those of the uncontrolled plant (for example, the B747

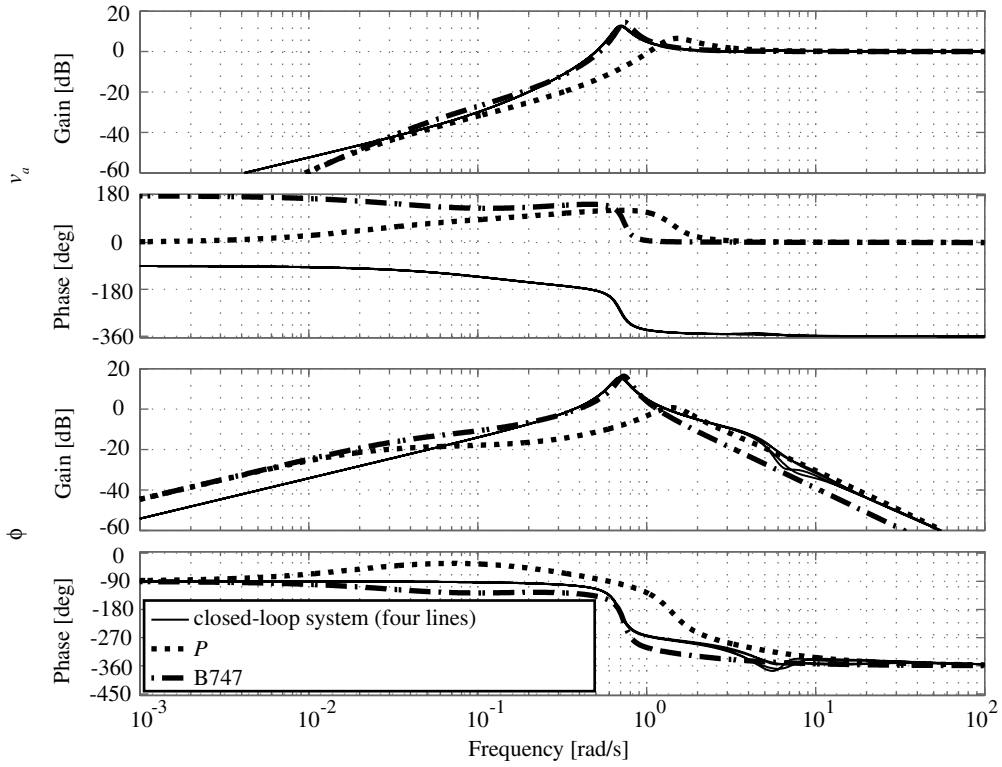

Fig. 7 Bode plots from v_g to v_a and ϕ with K_{opt} for the B747 model.

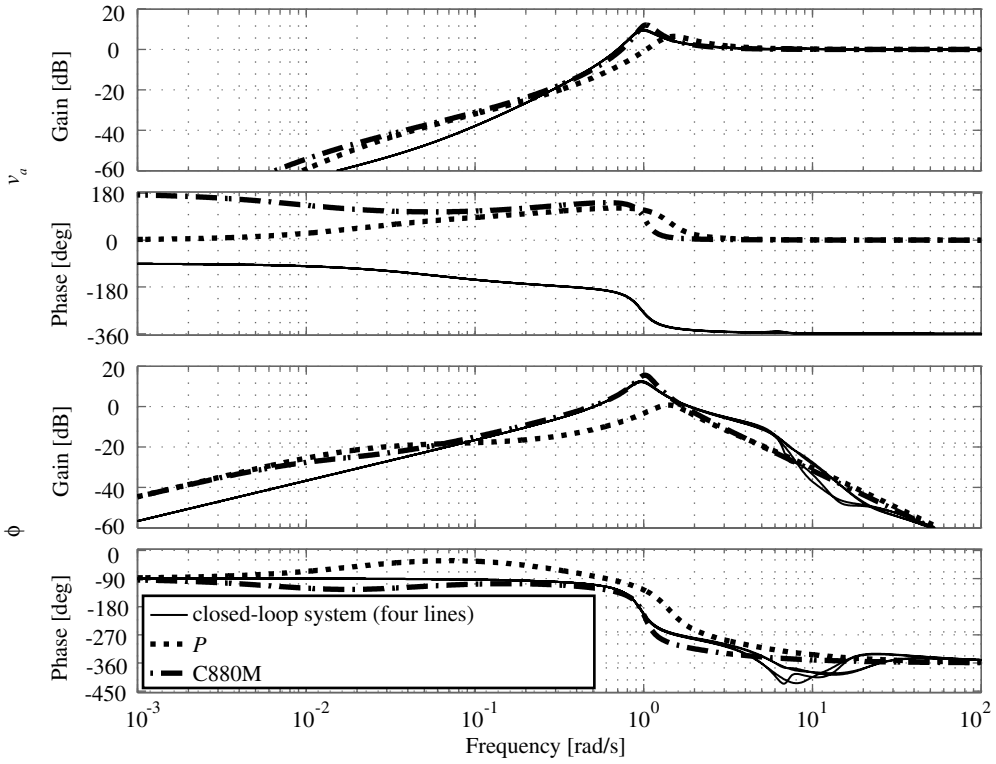

Fig. 8 Bode plots from v_g to v_a and ϕ with K_{opt} for the C880M model.

model, the C880M model and the uncontrolled plant, respectively, have 8.6-, 6.2-, and 4.6-s period Dutch-roll modes), the controlled plant with optimal feedback controller K_{opt} faithfully realizes the gains around the target aircraft's Dutch-roll mode frequencies; that is, the designed controllers have good model-matching performance over the frequency range of 0.2–2 rad/s for the prescribed uncertainties.

Numerical simulations, which are included in [25] and thus omitted here, with designed controllers confirm that the designed controllers almost realize the GR of their target aircraft.

3. *Feedforward Controller*

The feedforward controller F is now designed. The state-space matrices of P_n in Fig. 4 are given in the Appendix as Eq. (A2). The weighting function W_2 in Fig. 4 is set as follows:

$$W_2: \begin{cases} \frac{10}{s+0.10} I_2 \\ \frac{10}{s+0.10} I_2 \end{cases} \tag{18}$$

where the former weighting function is for the B747 model and the latter one is for the C880M model. These are set for F to satisfy inequalities (3–5) with the $\zeta(\omega)$ values specified in Table 1. With W_2 in Eq. (18), full-order (tenth-order) controllers F for the B747 and C880M models are designed setting the direct terms to be zeros. The state-space matrices of F are omitted for lack of space.

Figures 9 and 10 show the Bode plots of the cascaded system of the closed-loop system P_{cl}, the feedforward controller F, respectively, for the B747 and C880M models, and the target aircraft model $M_{z_m u_m}$ with a nominal delay-time set and four combinations of maximum and minimum aileron and rudder input delays (the plots are barely separable at the low frequencies). For reference, the Bode plots of the closed-loop system with the same nominal delay and the target aircraft model $M_{z_m u_m}$ are also given. These figures confirm that the designed controllers have good model-matching performance at low frequencies less than 2 rad/s for the prescribed uncertainties.

To verify the robust performance of F more rigorously, μ analysis is conducted. In Fig. 5, the uncertainty block $\tilde{\Delta}_F$ comprises Δ_u, which is composed of two real scalar blocks, and one 2×2 complex full block Δ_{p_F}. The results of μ analysis setting W_3 in Fig. 5 as W_2, which are included in [25] and thus omitted here, conclude that the feedforward controller F for the B747 and C880M models neither have robust performance defined by W_2 against the prescribed uncertainties. The results show that the upper μ has two peaks around the frequencies of the target aircraft's Dutch-roll mode and 6 rad/s. Considering these, the following weighting functions, which have low gains around the frequencies of the target aircraft's Dutch-roll mode compared with those at the low frequencies and sufficiently low gains over 2 rad/s, are next used for the μ analysis:

$$W_3: \begin{cases} \frac{14.945s^5+412.82s^4+2890.9s^3+4435.0s^2+2828.1s+1183.0}{s^7+30.096s^6+257.16s^5+675.13s^4+1058.3s^3+853.30s^2+187.06s+11.841} I_2 \\ \frac{14.837s^4+449.27s^3+3213.4s^2+3277.2s+3093.4}{s^6+32.056s^5+276.49s^4+550.72s^3+832.33s^2+403.06s+31.435} I_2 \end{cases} \tag{19}$$

where the former is for the B747 model and the latter is for the C880M model.

Using W_3 in Eq. (19) concludes that the feedforward controllers F for both models have robust performance, which is described in Tables 2 and 3, respectively, for the B747 and C880M models, using inequalities in Lemma 1 against the prescribed uncertainties. Although these results do not satisfy the design requirements for F,

Table 1 Guaranteed performance defined by Eq. (18)

Frequency, rad/s	$1/\zeta(\omega)$
0–0.1	0.02
0.1–1	0.1
1–2	0.2

Table 2 Guaranteed performance for F for the B747 model

Frequency, rad/s	$1/\zeta(\omega)$
0–0.13	0.02
0.13–0.39	0.1
0.39–0.59	0.2
0.59–2	0.28

Table 3 Guaranteed performance for F for the C880M model

Frequency, rad/s	$1/\zeta(\omega)$
0–0.15	0.02
0.15–0.60	0.1
0.60–1.09	0.2
1.09–2.0	0.28

the degradation is not so severe because the designed feedforward controllers are both confirmed to have robust right inverse performance against the prescribed uncertainties, as illustrated in Figs. 9 and 10. Thus, the designed feedforward controllers are adopted for our IFS controllers.

B. Experimental Results

IFS controllers are implemented in the MuPAL-α's onboard flight control computer. The feedforward controller F is implemented after discretization using a bilinear transform with 0.02 s. Noise-reduction filters

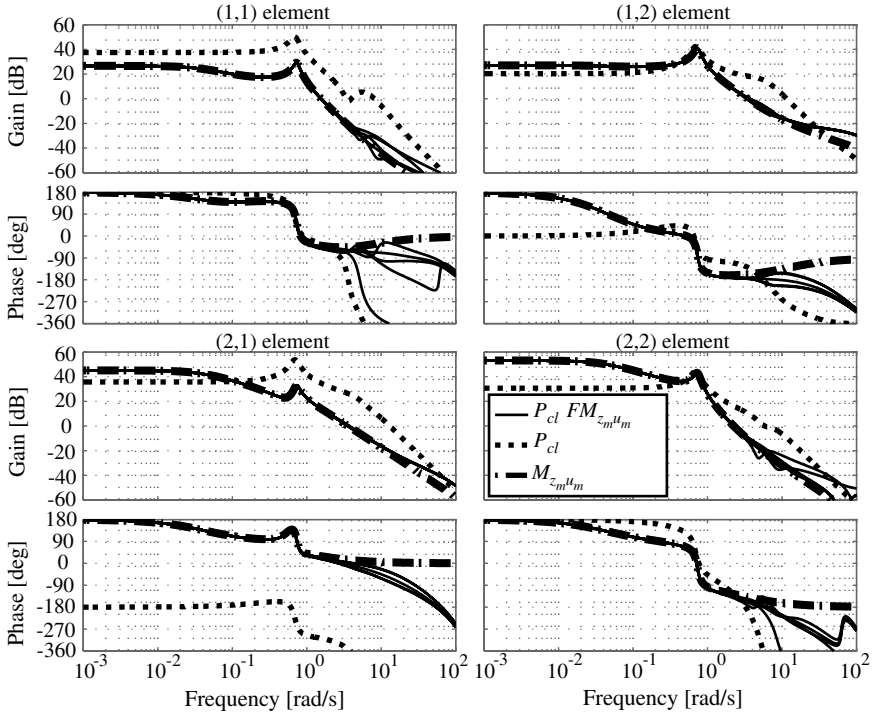

Fig. 9 Bode plots of $P_{cl}FM_{z_m u_m}$ for the B747 model. (Five lines are drawn for $P_{cl}FM_{z_m u_m}$.)

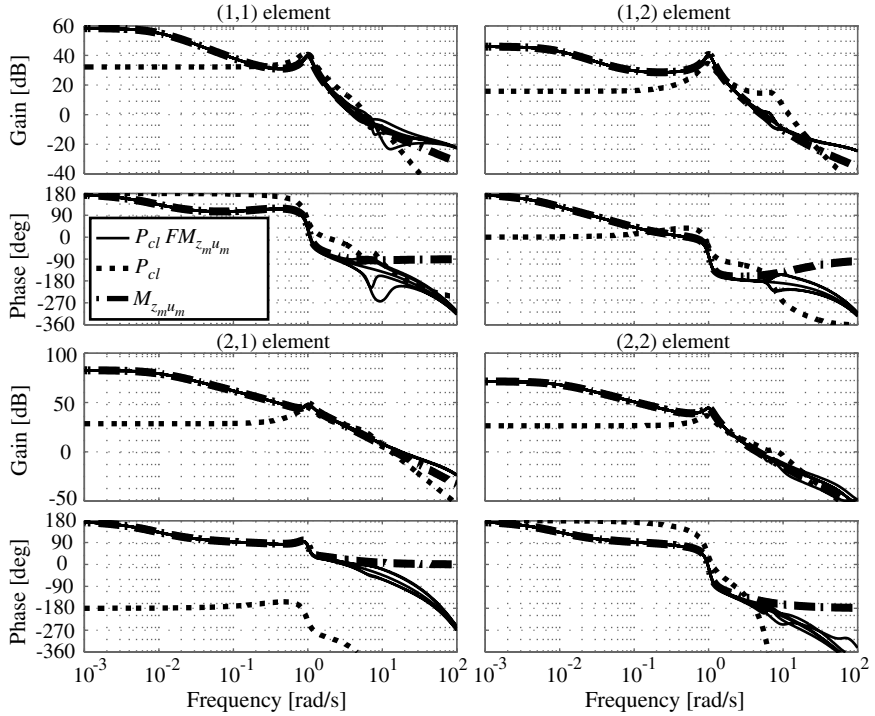

Fig. 10 Bode plots of $P_{cl}FM_{z_m u_m}$ for the C880M model. (Five lines are drawn for $P_{cl}FM_{z_m u_m}$.)

$$F_1\colon \frac{1}{(0.03s+1)^3} I_2 \qquad F_2\colon \frac{1}{0.02s+1} I_4$$

which are, respectively, for u_m and y, and $M_{z_m u_m}$ are implemented after discretization using a zero-order hold with 0.02 s.

1. HIL Simulation

Before carrying out flight tests of the controllers, HIL simulations, in which the motions of MuPAL-α simulating the target aircraft using the implemented IFS controllers are calculated using six-degree-of-freedom nonlinear equations for the original aircraft, were conducted to check controller performance.

First, GR realization performance was checked. Figures 11 and 12 show HIL GR simulation results for the B747 and C880M IFS controllers, respectively, for a step gust input shown in the uppermost plot row. In these simulations, the GR of the target aircraft model was computed offline using the recorded gust inputs because the GR of the target aircraft model is not calculated online in our IFS controllers (see Fig. 1). For comparison, GR numerical simulation results of uncontrolled MuPAL-α using the recorded gust inputs is also shown (aileron and rudder deflections for the uncontrolled MuPAL-α are omitted because they are set as zeros). These figures confirm the following: First, comparison between the GR of the target aircraft models and the uncontrolled MuPAL-α indicates that some IFS controller is needed to realize GR of the target aircraft models with

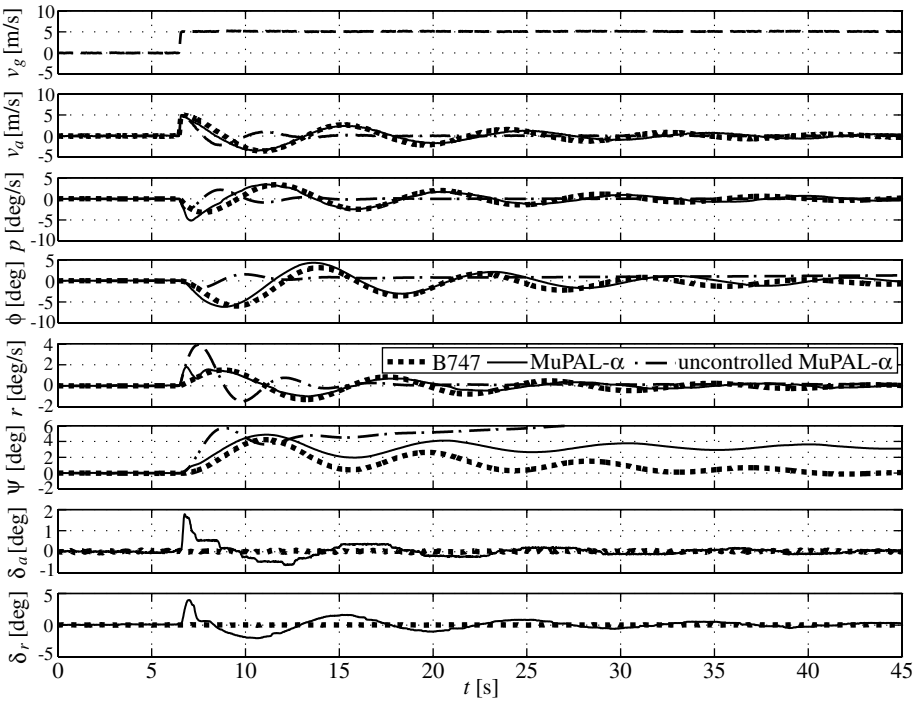

Fig. 11 Step-type gust response in HIL simulation with IFS controller for the B747 model.

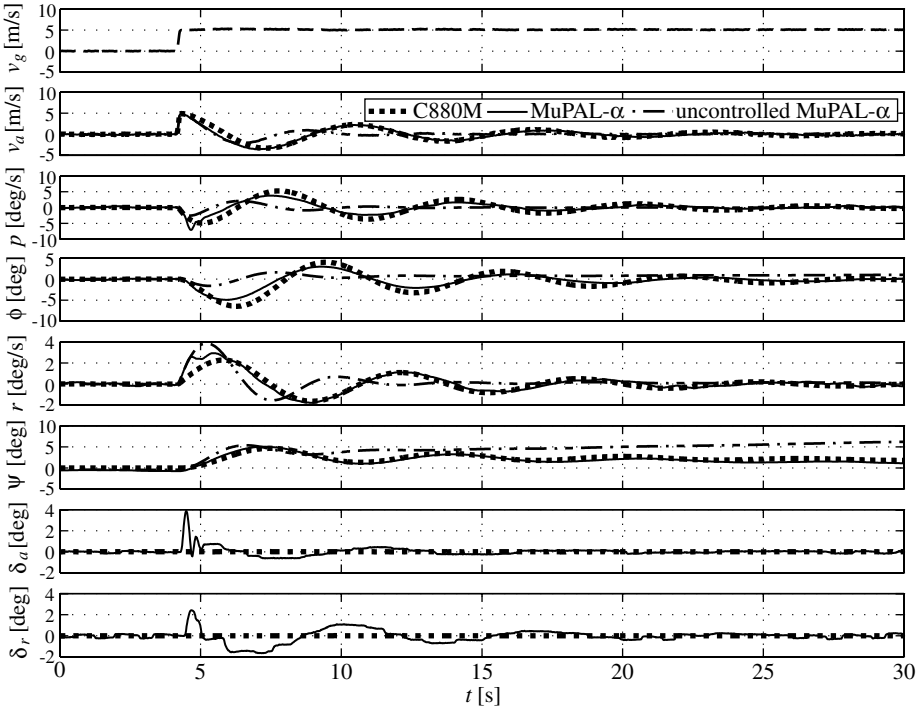

Fig. 12 Step-type gust response in HIL simulation with IFS controller for the C880M model.

MuPAL-α. Second, although there are some discrepancies between MuPAL-α's response and the target aircraft response for both target aircraft models, the amplitudes and period of v_a and ϕ of the Dutch-roll mode of MuPAL-α simulating the target aircraft are almost the same as those of the corresponding model; that is, our designed controllers almost realize the GR of the target aircraft models.

Next, HR realization performance was checked. Doublet inputs to both ailerons and rudder (B747 model) and rudder only (C880M model) are applied to excite oscillation. Figures 13 and 14 show HIL HR simulation results for IFS controllers for the B747 and C880M models, respectively. For comparison, HR numerical simulation results of the uncontrolled MuPAL-α using the recorded model inputs is also shown (aileron and rudder deflections for the uncontrolled MuPAL-α are omitted because they are set the same as those of the models). These figures confirm the following: First, comparison between HR of the target models and the uncontrolled MuPAL-α indicates that some IFS controller is needed to realize HR of the target aircraft models with MuPAL-α. Second, there are hardly any discrepancies between MuPAL-α's response and the target aircraft outputs; that is, our designed controllers realize the HR of the corresponding target aircraft models with high fidelity.

Although the aileron inputs are set to zero for the C880M model, our IFS controller uses only the target aircraft outputs, not actual inputs, and so the HR of the target aircraft with aileron input is also realized, as will be shown in the following flight-test results.

2. *Flight Test*

After HIL simulation tests, the IFS controllers were tested in actual flight. Figures 15 and 16 show time histories of the IFS controllers, respectively, for the B747 and C880M models under manual pilot input. As in Figs. 11 and 12, the model outputs are computed offline with a simple gust estimate ($v_g = v_a - v_i$), which is shown in the

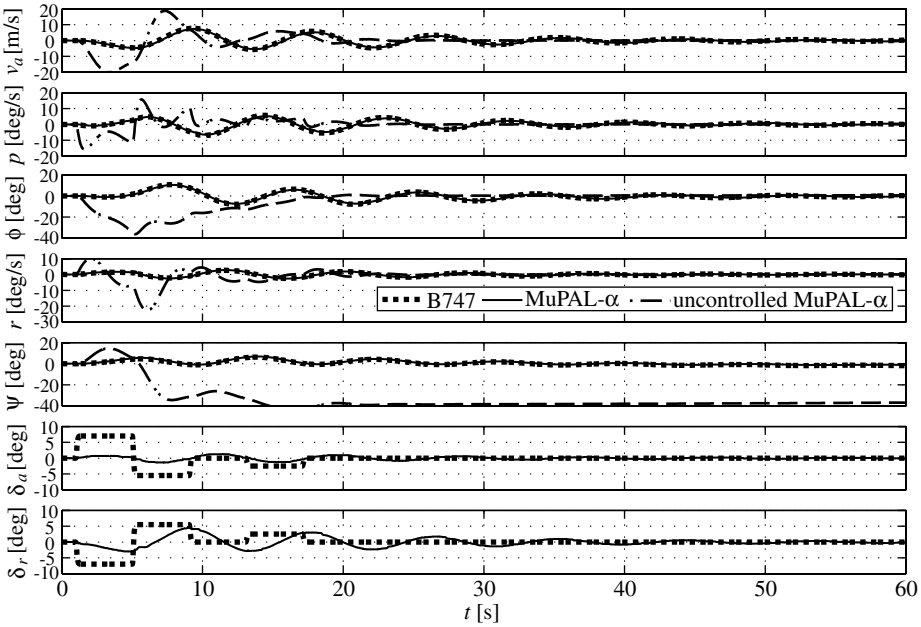

Fig. 13 Handling response in HIL simulation with IFS controller for the B747 model.

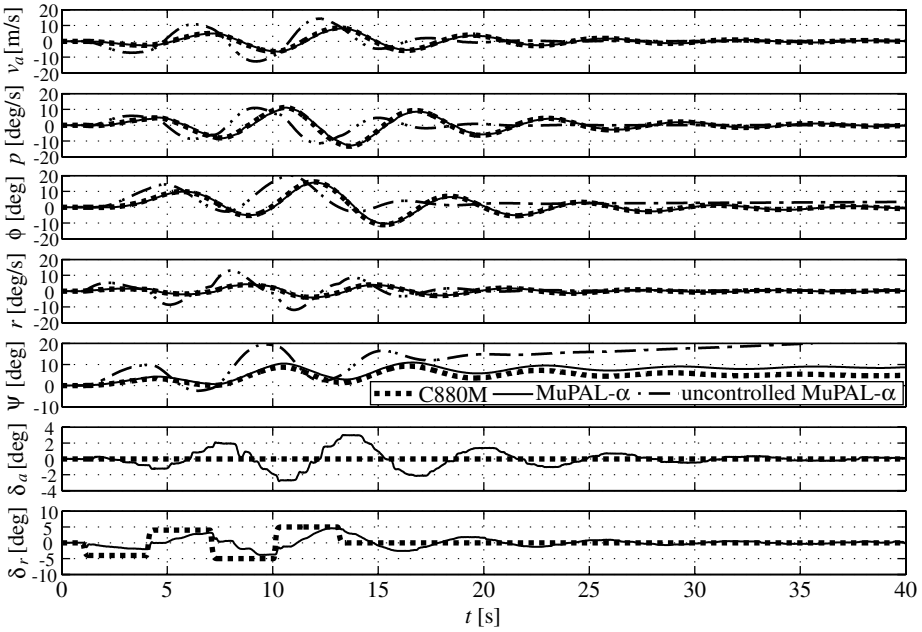

Fig. 14 Handling response in HIL simulation with IFS controller for the C880M model.

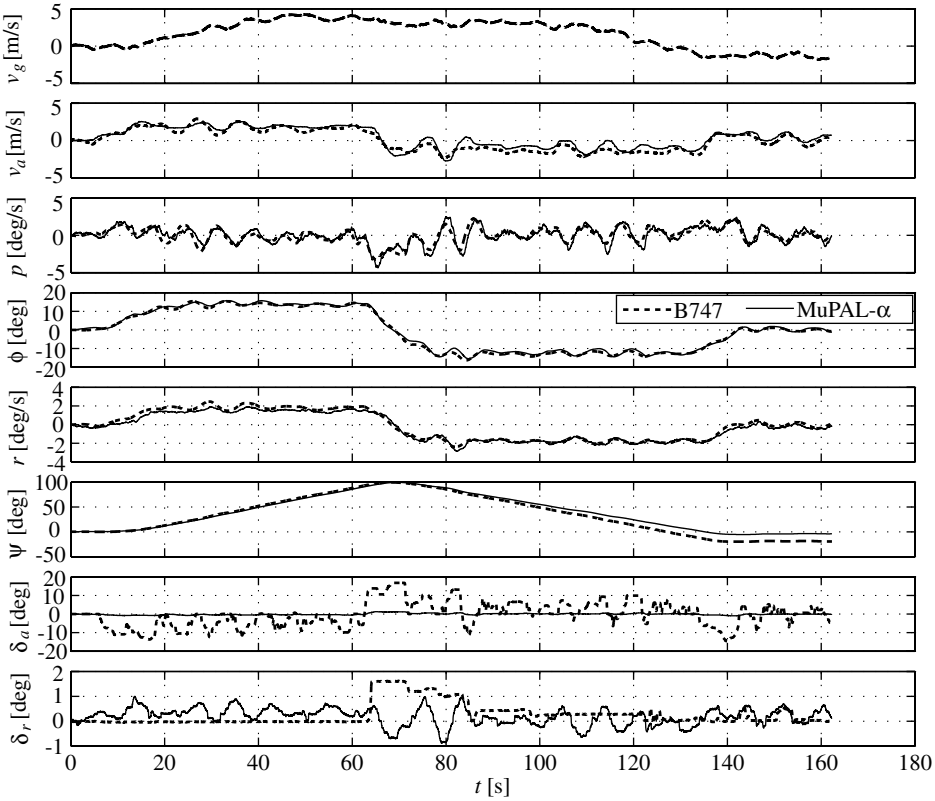

Fig. 15 Time histories of flight test for IFS controller for the B747 model.

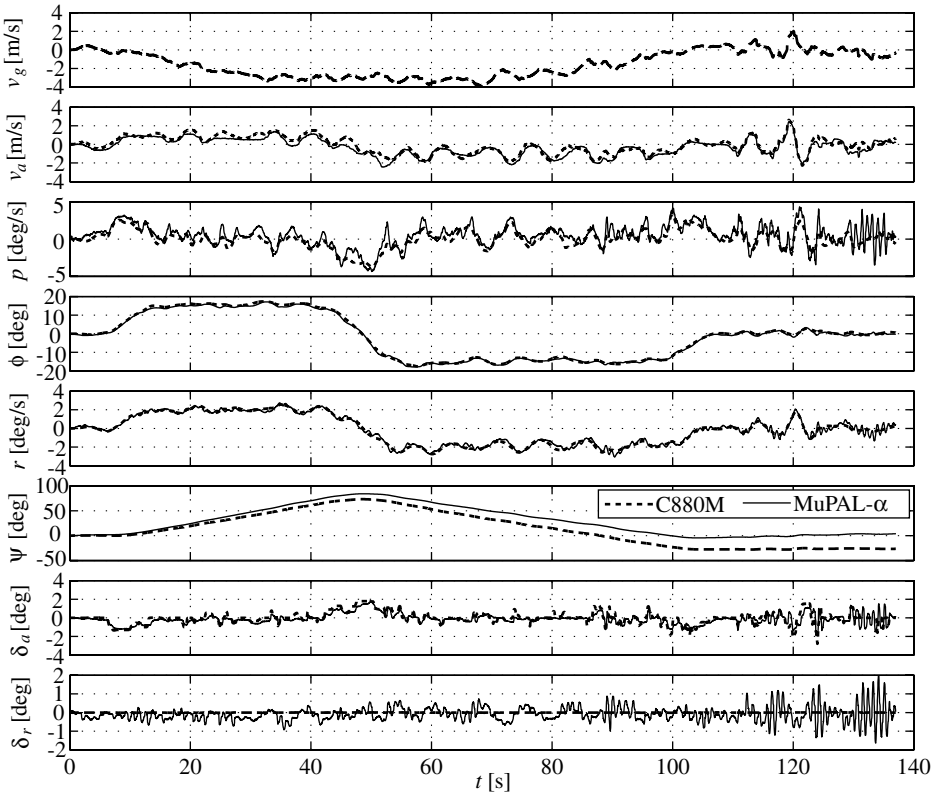

Fig. 16 Time histories of flight test for IFS controller for the C880M model.

uppermost plot row, and the same pilot inputs. In these figures, two different lines are drawn; however, they sometimes overlap and it is difficult to discriminate between them in such case, which consequently indicates good model-matching performance of our designed controllers. Although there are some discrepancies between MuPAL-α and the target aircraft outputs for both target models, the lateral air velocity and roll angle of MuPAL-α are almost the same as those of the models; that is, our designed controllers almost realize the GR as well as the HR of the target aircraft in real flight.

In Fig. 16, oscillatory inputs are shown in MuPAL-α rudder deflection. The cause of this phenomenon has not been identified; however, because HIL simulations and numerical simulations both show that our designed controllers have good performance, the rudder oscillation may be caused by modeling errors. Thus, for better IFS controllers, more precise model of the original aircraft may be required.

IV. IFS Controller for Handling-Quality Investigation

One of our primary research applications for MuPAL-α is evaluating aircraft handling qualities in actual flight. In flight, encountering wind gusts is inevitable, but for pure handling-quality investigations, the effects of gusts on aircraft motions must be minimized as much as possible. Furthermore, it is preferable to explore as great a range of maneuverability as possible in a single flight because the flight conditions for each maneuver need to be as identical as possible. Considering these conditions, we obtain the following design requirements for IFS controllers for handling-quality investigation: 1) as much gust alleviation as possible and 2) a wide range of maneuverability within a single controller design.

These requirements are realized by the design framework presented in Sec. II by setting $M_{z_m w_g}$ to be $\mathbf{0}$ and $M_{z_m u_m}$ to be the model that defines the maneuverability to be tested, because the transfer function of the cascaded system $P_{\mathrm{cl}}F$ is approximately described as an identity matrix at low frequencies; that is, z_p reproduces z_m for the low-frequency components. In this section, the details of designing controllers K and F are described and experimental results are shown.

A. Controller Design

The controller design framework in this section is almost the same as that in the previous section, and so duplicate descriptions are omitted. The L/D motion model of MuPAL-α, the actuator model, and the uncertainties are the same as those used in the previous section. In this section, $M_{z_m w_g}$ is set as follows:

$$M_{z_m w_g}: \begin{bmatrix} v_a \\ \phi \end{bmatrix} = \mathbf{0} v_g \tag{20}$$

In other words, the target aircraft completely eliminates the response to gusts. Although complete elimination of the GR is impossible in practice, using the $M_{z_m w_g}$ in Eq. (20) produces an IFS controller that suppresses GR as much as possible. In this section, $M_{z_m u_m}$ is not determined a priori because it depends heavily on the objective of the handling-quality investigation.

1. Feedback Controller

The weighting function for model-matching performance W_1 in Fig. 3 is set as follows:

$$W_1: \gamma I_2 \tag{21}$$

This weighting function is set for the IFS controller to suppress the gust response at all frequencies.

After applying Algorithm 1 in which $M_{z_m w_g}$ is set as $\mathbf{0}$, W_1 is set as Eq. (21), matrices P and X are set to belong to $\mathcal{S}^8$, and the rank constraint in Eq. (12b) is replaced by

$$\operatorname{rank} \begin{bmatrix} P & \mathbf{I} \\ \mathbf{I} & X \end{bmatrix} = 8$$

the obtained maximum γ is 0.80312. The corresponding controller K_{opt} and the scaling matrix S are as follows:

$$K_{\mathrm{opt}} = \begin{bmatrix} -5.0024 \times 10^{-3} & 0.68915 & 1.5021 & 0.60948 \\ -2.1869 \times 10^{-2} & -0.60614 & -0.42949 & 2.8331 \end{bmatrix}$$

$$S = 10^{-2} \times \mathtt{diag}(3.9603, 1.3490, 1.1928 \times I_2)$$

Figure 17 shows the Bode plots of the closed-loop system and the uncontrolled plant from v_g to v_a and ϕ. As in Figs. 7 and 8, four lines for the closed-loop system are drawn, although they mostly overlap. Although the designed controller cannot completely suppress the gust response, in contrast to $M_{z_m w_g}$ in Eq. (20), the figure confirms that the peak gains are well depressed: from 6.94 dB at 1.51 rad/s to 1.53 dB at 6.74 rad/s for v_a and from 0.776 dB at 1.41 rad/s to -14.0 dB at 4.77 rad/s for ϕ. A gain increase in ϕ of the closed-loop system is seen over the range 4–20 rad/s, but the peak gain is lower than that of the uncontrolled plant.

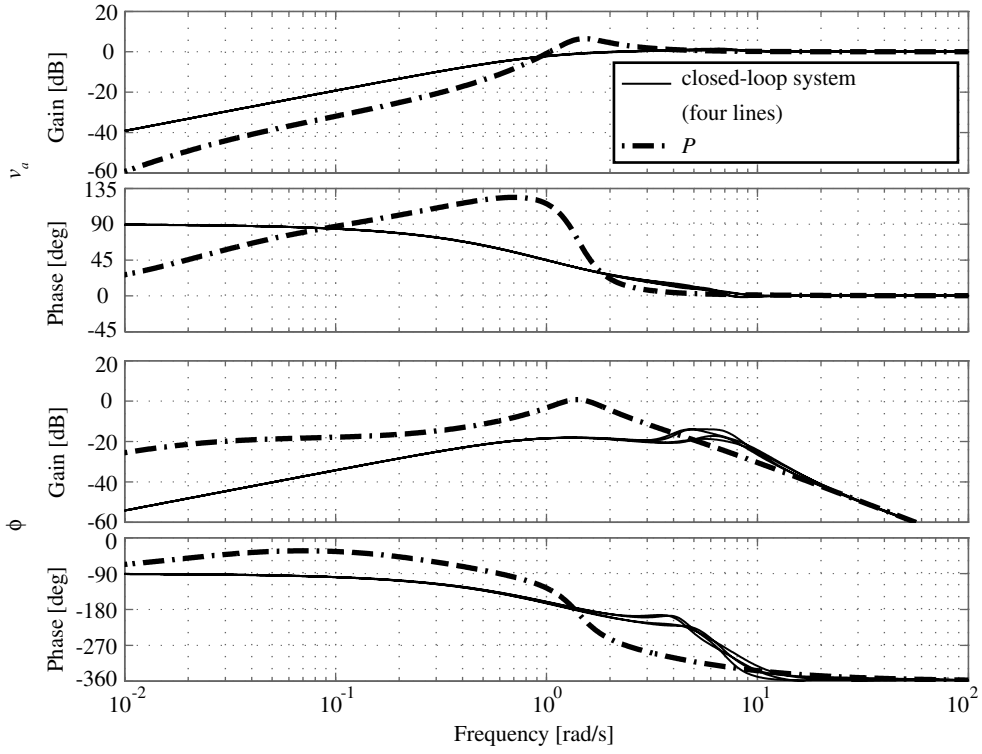

Fig. 17 Bode plots from v_g to v_a and ϕ with K_{opt} for Eq. (20).

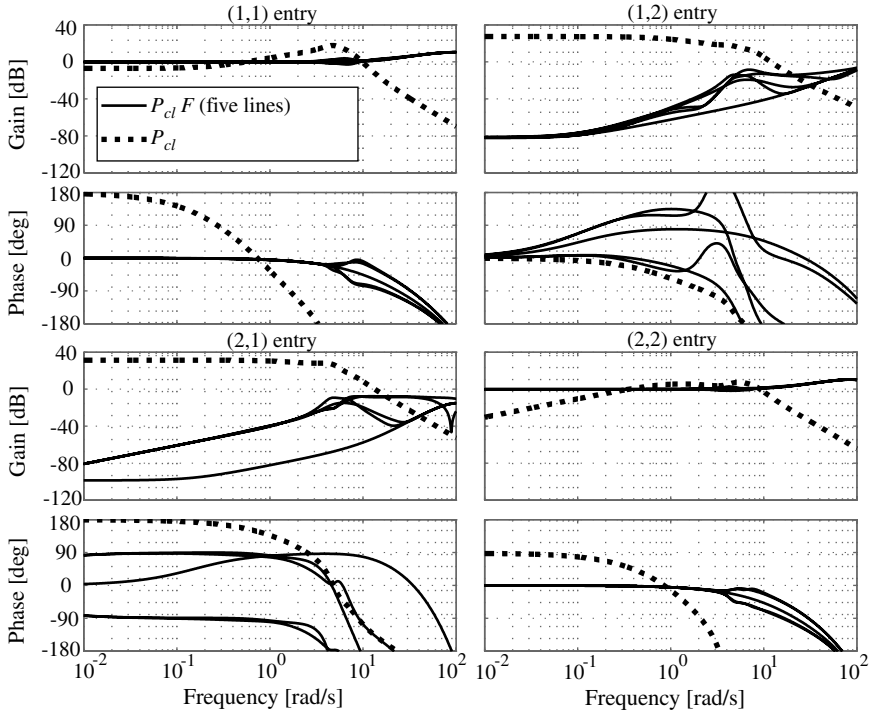

Fig. 18 Bode plots of the cascaded system $P_{\mathrm{cl}}F$.

Numerical simulation with our design controller, which is included in [26] and thus omitted here, confirms that the controller depresses the overshoots and reduces the settling time compared with the uncontrolled plant.

2. Feedforward Controller

Next, the feedforward controller F is designed to realize a wide range of maneuverability. The weighting function W_2 in Fig. 4 is the same as in the previous section; that is, W_2 is set as

$$\frac{10}{s+0.10}I_2$$

A full-order (tenth-order) controller F with the direct terms set to be zeros is designed. The state-space matrices are omitted for lack of space.

Figure 18 shows the Bode plots of the cascaded system of the closed-loop system P_{cl} and F with a nominal delay-time set and four combinations of maximum and minimum delay times of aileron and rudder inputs. For comparison, the Bode plots of P_{cl} with the nominal delay are also drawn. This figure confirms that at the low frequencies ($\omega \leq 2$ rad/s), the cascaded system $P_{\mathrm{cl}}F$ exhibits the following characteristics: the gains of diagonal elements are almost unity, the phase deviations of diagonal elements from zeros are very small, and the gains of nondiagonal elements are very small. Although the phase deviations of nondiagonal elements from zeros are very large, the gains are very small and so their effects are negligible for these frequencies. These results confirm that F works as a filtered right inverse system of the closed-loop system; that is, a variety of HR is realized by simply exchanging $M_{z_m u_m}$.

As in the previous section, μ analysis is conducted to rigorously verify the robust performance of F. The results of μ analysis setting W_3 in Fig. 5 as W_2 cannot conclude that the designed controller F has robust performance defined by W_2 against the prescribed uncertainties. However, using the following W_3 in Eq. (22) concludes that the controller F has robust performance, which is described in Table 4 using inequalities in Lemma 1, against the prescribed uncertainties.

$$W_3\colon \frac{29.126}{s^3+1.8374s^2+3.5545s+0.28863}I_2 \qquad (22)$$

The guaranteed performance against the prescribed uncertainties does not meet the design requirements, but the shortfall is not so severe. Thus, it was decided to proceed with using the designed feedforward controller in the subsequent experiments.

B. Experimental Results

As in the previous section, the feedforward controller F was implemented in MuPAL-α's onboard flight control computer after discretization by a bilinear transformation with 0.02 s, and the same filters F_1 and F_2 were implemented after discretization by a zero-order hold with 0.02 s.

Because $M_{z_m u_m}$ heavily depends on the objective of the handling-quality investigation and the details of future investigations have not yet been determined, in this paper, the following simple two models are used as $M_{z_m u_m}$ to verify IFS controller performance:

Model 1:

$$z_m = \frac{1}{(s+1)^2}\begin{bmatrix} 0 & 1 \\ -1 & 0 \end{bmatrix} u_m \qquad (23)$$

Model 2:

$$z_m = \begin{bmatrix} 0 & \frac{0.5^2}{s^2+0.3s+0.5^2} \\ \frac{-1}{s^2+0.6s+1} & \end{bmatrix} u_m \qquad (24)$$

where $z_m = [v_a\ \phi]^T$ and $u_m = [\delta_a\ \delta_r]^T$.

As with the IFS controllers for the B747 and C880M models, HIL simulations are first conducted to confirm GR suppression performance and HR realization performance of our designed controller. For lack of space, only GR suppression result is shown in Fig. 19 (other results are included in [26]). Those figures confirm the

Table 4 Guaranteed performance defined by Eq. (22)

Frequency, rad/s	$1/\zeta(\omega)$
0–0.14	0.02
0.14–0.96	0.1
0.96–1.81	0.2
1.81–2	0.25

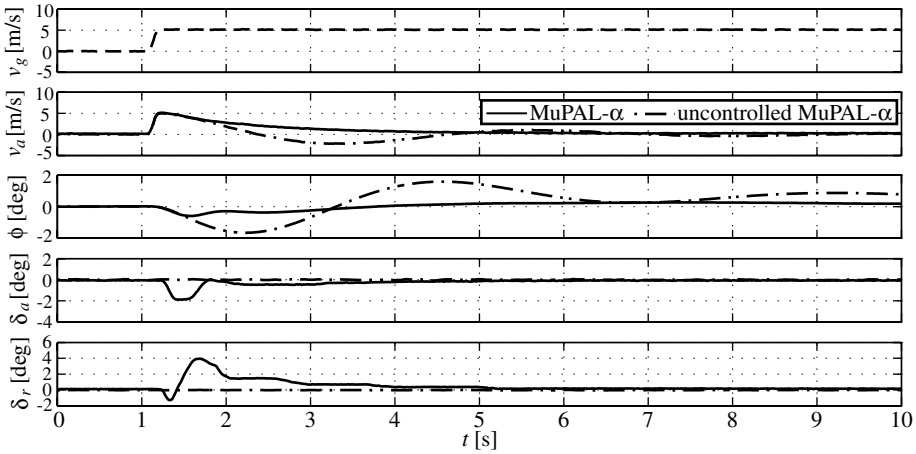

Fig. 19 Step-type gust response in HIL simulation.

following: the designed IFS controller depresses the overshoot and shortens the settling time, which is shown in Fig. 19, and it realizes HR defined by $M_{z_m u_m}$ with high fidelity. Thus, we proceed to the flight tests of the IFS controller. During the flight tests the atmospheric conditions were very calm and so GR suppression performance could not be verified directly. However, it was indirectly confirmed, as explained next.

Figures 20 and 21 show the flight-test results for aileron and rudder doublet inputs for models 1 and 2, respectively. These confirm that z_p faithfully coincide with z_m, directly showing high HR fidelity. These

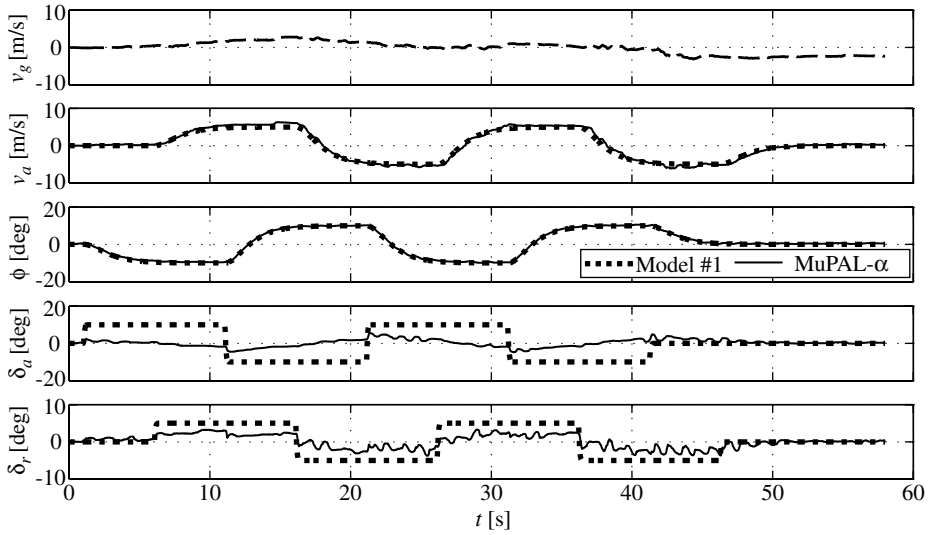

Fig. 20 Time histories of flight test using model 1.

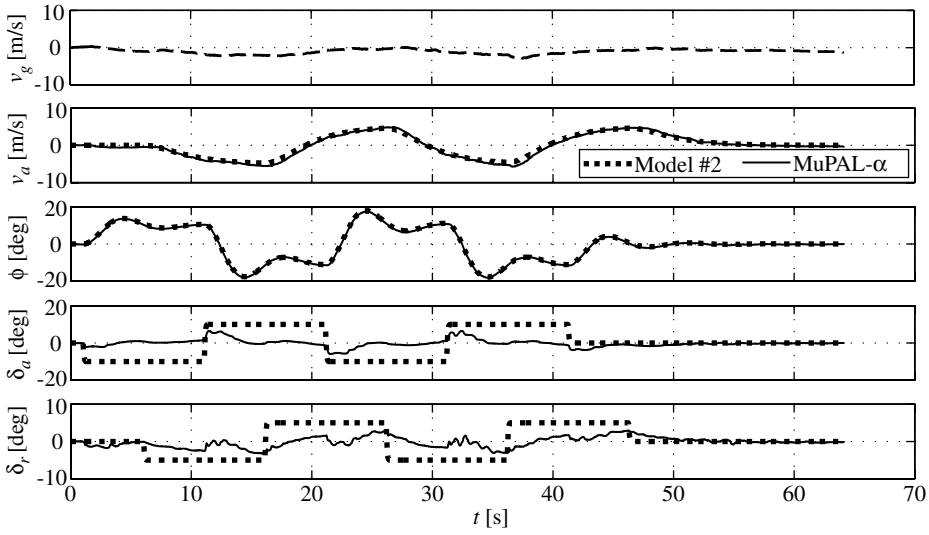

Fig. 21 Time histories of flight test using model 2.

results also indirectly confirm good GR suppression, because if this were not the case, then z_m would differ from z_p, which can barely be seen in these figures.

Flight-test results for model 1 with manual pilot inputs and several related pilot comments are included in [26]. In the flight test, our IFS controller faithfully achieves HR defined by $M_{z_m u_m}$, although the maximum roll angle reaches about 45 deg.

V. Conclusions

This paper proposes a new controller framework for in-flight simulator (IFS) controllers to realize gust response (GR) and handling response (HR) of a target aircraft simultaneously. The controller is a two-degree-of-freedom model-matching controller and is designed by the following sequence: the feedback controller, which aims to vary GR characteristics, is first designed via the H_∞ model-matching approach considering plant uncertainties, then the feedforward controller, which aims to vary HR characteristics, is designed via the H_∞ approach. Although the feedforward controller is designed without considering plant uncertainties, its robust performance against the plant uncertainties is confirmed via μ analysis a posteriori.

Using the proposed method, IFS controllers for the lateral–directional (L/D) motions of a research aircraft for two different real target aircraft models, a Boeing 747 and a Convair 880M, are designed and are confirmed by hardware-in-the-loop (HIL) simulations and flight tests to achieve the simultaneous realization of HR and GR of the target aircraft.

In addition, an IFS controller for handling-quality investigation for L/D motions is designed, with the design requirements of gust response suppression to as great an extent as possible and realizing a wide range of maneuverability by simply exchanging models that define the maneuverability to be tested. HIL simulations and flight tests confirm that the designed controller well suppresses gust effect and achieves the maneuverability defined by the model.

These experimental results demonstrate the applicability of our proposed method for IFS controller design.

Appendix: State-Space Matrices of MuPAL-α and Models

The state-space matrices

$$\begin{bmatrix} A & B \\ C & D \end{bmatrix}$$

of P in Fig. 6 are as follows:

$$\left[\begin{array}{cccccccccccc}
-0.17810 & 6.0791 & 9.7633 & -65.623 & 0 & 2.8900 & 0 & 0 & -0.17810 & 0 & 0 & 0 & 0 \\
-0.057500 & -3.8100 & 0 & 1.3430 & -10.750 & 1.1870 & 0 & 0 & -0.057500 & 0 & 0 & 0 & 0 \\
0 & 1.0000 & 0 & 0.094352 & 0 & 0 & 0 & 0 & 0 & 0 & 0 & 0 & 0 \\
0.025300 & -0.062800 & 0 & -0.47500 & 0.34500 & -2.2200 & 0 & 0 & 0.025300 & 0 & 0 & 0 & 0 \\
0 & 0 & 0 & 0 & -5.2632 & 0 & 3.7895 & 0 & 0 & 0 & 0 & -3.7895 & 0 \\
0 & 0 & 0 & 0 & 0 & -14.286 & 0 & 11.000 & 0 & 0 & 0 & 0 & -11.000 \\
0 & 0 & 0 & 0 & 0 & 0 & -18.750 & 0 & 0 & 1.0000 & 0 & 37.500 & 0 \\
0 & 0 & 0 & 0 & 0 & 0 & 0 & -18.750 & 0 & 0 & 1.0000 & 0 & 37.500 \\
1.0000 & 0 & 0 & 0 & 0 & 0 & 0 & 0 & 1 & 0 & 0 & 0 & 0 \\
0 & 0 & 57.296 & 0 & 0 & 0 & 0 & 0 & 0 & 0 & 0 & 0 & 0 \\
0 & 0 & 0 & 0 & 0 & 0 & -6.2500 & 0 & 0 & 0 & 0 & 12.500 & 0 \\
0 & 0 & 0 & 0 & 0 & 0 & 0 & -6.2500 & 0 & 0 & 0 & 0 & 12.500 \\
1 & 0 & 0 & 0 & 0 & 0 & 0 & 0 & 1 & 0 & 0 & 0 & 0 \\
0 & 1 & 0 & 0 & 0 & 0 & 0 & 0 & 0 & 0 & 0 & 0 & 0 \\
0 & 0 & 1 & 0 & 0 & 0 & 0 & 0 & 0 & 0 & 0 & 0 & 0 \\
0 & 0 & 0 & 1 & 0 & 0 & 0 & 0 & 0 & 0 & 0 & 0 & 0
\end{array}\right] \tag{A1}$$

where the states, the inputs, and the outputs are, respectively,

$$[v_i\ (\mathrm{m/s})\ p\ (\mathrm{rad/s})\ \phi\ (\mathrm{rad})\ r\ (\mathrm{rad/s})\ \delta_a\ (\mathrm{rad})\ \delta_r\ (\mathrm{rad})\ x_d^T]^T$$

$$[v_g\ (\mathrm{m/s})\ w_d^T\ \delta_{a_c}\ (\mathrm{rad})\ \delta_{r_c}\ (\mathrm{rad})]^T$$

and

$$[v_a\ (\mathrm{m/s})\ \phi\ (\mathrm{deg})\ z_d^T\ v_a\ (\mathrm{m/s})\ p\ (\mathrm{rad/s})\ \phi\ (\mathrm{rad})\ r\ (\mathrm{rad/s})]^T$$

Here, $x_d \in \mathcal{R}^2$, $w_d \in \mathcal{R}^2$, and $z_d \in \mathcal{R}^2$, respectively, denote the state, the exogenous input, and the exogenous output to define the delay model in Eq. (7). Thus, they do not have their units because they are not actually existing variables.

The state-space matrices

$$\begin{bmatrix} A & B \\ C & D \end{bmatrix}$$

of P_n are as follows:

$$\begin{bmatrix}
-0.17810 & 6.0791 & 9.7633 & -65.623 & 0 & 2.8900 & 0 & 0 & 0 & 0 \\
-0.057500 & -3.8100 & 0 & 1.3430 & -10.750 & 1.1870 & 0 & 0 & 0 & 0 \\
0 & 1.0000 & 0 & 0.094352 & 0 & 0 & 0 & 0 & 0 & 0 \\
0.025300 & -0.062800 & 0 & -0.47500 & 0.34500 & -2.2200 & 0 & 0 & 0 & 0 \\
0 & 0 & 0 & 0 & -5.2632 & 0 & 3.7895 & 0 & -3.7895 & 0 \\
0 & 0 & 0 & 0 & 0 & -14.286 & 0 & 11.000 & 0 & -11.000 \\
0 & 0 & 0 & 0 & 0 & 0 & -16.667 & 0 & 33.333 & 0 \\
0 & 0 & 0 & 0 & 0 & 0 & 0 & -16.667 & 0 & 33.333 \\
1.0000 & 0 & 0 & 0 & 0 & 0 & 0 & 0 & 0 & 0 \\
0 & 0 & 57.296 & 0 & 0 & 0 & 0 & 0 & 0 & 0 \\
1 & 0 & 0 & 0 & 0 & 0 & 0 & 0 & 0 & 0 \\
0 & 1 & 0 & 0 & 0 & 0 & 0 & 0 & 0 & 0 \\
0 & 0 & 1 & 0 & 0 & 0 & 0 & 0 & 0 & 0 \\
0 & 0 & 0 & 1 & 0 & 0 & 0 & 0 & 0 & 0
\end{bmatrix} \tag{A2}$$

where the states are the same as in Eq. (A1), the inputs are $[\delta_{a_c}\ (\text{rad})\ \delta_{r_c}\ (\text{rad})]^T$, and the outputs are

$$[v_a\ (\text{m/s})\ \phi\ (\text{deg})\ v_a\ (\text{m/s})\ p\ (\text{rad/s})\ \phi\ (\text{rad})\ r\ (\text{rad/s})]^T$$

Note that $v_a = v_i$ holds because we now ignore gust v_g.

The state-space matrices

$$\begin{bmatrix} A & B \\ C & D \end{bmatrix}$$

of $M_{z_m u_m}$ are as follows:

For the B747 model:

$$\begin{bmatrix}
-8.9000 \times 10^{-2} & 9.9566 & 9.6989 & -66.621 & 0 & 0.99694 \\
-1.9744 \times 10^{-2} & -0.97500 & 0 & 0.32700 & -0.22700 & 0.063600 \\
0 & 1.0000 & 0 & 0.14945 & 0 & 0 \\
2.4940 \times 10^{-3} & -0.16600 & 0 & -0.21700 & -0.026400 & -0.15100 \\
1 & 0 & 0 & 0 & 0 & 0 \\
0 & 0 & 57.296 & 0 & 0 & 0
\end{bmatrix} \tag{A3}$$

For the C880M model:

$$\begin{bmatrix}
-0.13900 & 6.2432 & 9.7663 & -68.601 & 2.5556 & 1.7221 \\
-0.046309 & -1.3900 & 0 & 0.98000 & -3.8400 & 0.33500 \\
0 & 1.0000 & 0 & 0.091007 & 0 & 0 \\
7.2440 \times 10^{-3} & -0.11300 & 0 & -0.21500 & -0.40100 & -0.32700 \\
1 & 0 & 0 & 0 & 0 & 0 \\
0 & 0 & 57.296 & 0 & 0 & 0
\end{bmatrix} \tag{A4}$$

where the states are $[v_i\ (\text{m/s})\ p\ (\text{rad/s})\ \phi\ (\text{rad})\ r\ (\text{rad/s})]^T$, the inputs are $[\delta_a\ (\text{rad})\ \delta_r\ (\text{rad})]^T$, and the outputs are $[v_a\ (\text{m/s})\ \phi\ (\text{deg})]^T$.

The state-space matrices A, B, C, and D of $M_{z_m w_g}$ are, respectively, given as A, the first column of A, C, and the first column of C, with matrices A, B, etc., in Eq. (A3) or Eq. (A4), where the states are the same as in Eq. (A3) or Eq. (A4), the input is v_g m/s, and the outputs are the same as in Eq. (A3) or Eq. (A4).

References

[1] Weingarten, N. C., "History of In-Flight Simulation at General Dynamics," *Journal of Aircraft*, Vol. 42, No. 2, 2005, pp. 290–298. doi:10.2514/1.4663

[2] Motyka, P. R., Rynaski, E. G., and Reynolds, P. A., "Theory and Flight Verification of the TIFS Model-Following System," *Journal of Aircraft*, Vol. 9, No. 5, 1972, pp. 347–353.

[3] Komoda, M., Kawahata, N., Tsukano, Y., and Ono, T., "VSRA In-Flight Simulator—Its Evaluation and Applications," AIAA Paper 88-4605, Sept. 1988.

[4] Hanke, D., and Lange, H. H., "Flight Evaluation of the ATTAS Digital Fly-By-Wire/Light Flight Control System," *Proceedings of ICAS 16th Congress*, International Council of the Aeronautical Sciences, Stockholm, Sweden, 1988, pp. 866–876.

[5] Sato, M., "Flight Test of Model-Matching Controller for In-Flight Simulator MuPAL-α," *Journal of Guidance, Control, and Dynamics*, Vol. 29, No. 6, 2006, pp. 1476–1481. doi:10.2514/1.25685

[6] Kawahata, N., "Model-Following System with Assignable Error Dynamics and Its Application to Aircraft," *Journal of Guidance, Control, and Dynamics*, Vol. 3, No. 6, 1980, pp. 508–516.

[7] Adams, R. J., Buffington, J. M., Sparks, A. G., and Banda, S. S., "Robust Multivariable Flight Control," *Advances in Industrial Control*, Springer–Verlag, London, 1994, pp. 56–68 and 128–141.

[8] Yang, C. D., Ouyang, J., and Ju, H. S., "Pilot Prefilter Design via H_∞ Model-Matching Approach," *Journal of Guidance, Control, and Dynamics*, Vol. 20, No. 1, 1997, pp. 186–189.

[9] Balas, G. J., Packard, A. K., Renfrow, J., Mullaney, C., and M'Closkey, R. T., "Control of the F-14 Aircraft Lateral–Directional Axis During Powered Approach," *Journal of Guidance, Control, and Dynamics*, Vol. 21, No. 6, 1998, pp. 899–908.

[10] Hyde, R. A., "An H_∞ Loop-Shaping Design for the VAAC Harrier," *Flight Control Systems: Practical Issues in Design and Implementation*, Inst. of Electrical Engineers, Stevenage, England, U.K., 2000, pp. 348–376.

[11] Papageorgiou, G., and Glover, K., "Two-Degree-of-Freedom Control of an Actively Controlled Wind-Tunnel Model," *Journal of Guidance, Control, and Dynamics*, Vol. 25, No. 3, 2002, pp. 510–516.

[12] Prempain, E., and Postlethwaite, I., "Static H_∞ Loop Shaping Control of a Fly-by-Wire Helicopter," *Automatica*, Vol. 41, 2005, pp. 1517–1528.
doi:10.1016/j.automatica.2005.04.001

[13] Yu, W., and Sobel, K. M., "Robust Eigenstructure Assignment with Structured State Space Uncertainty," *Journal of Guidance, Control, and Dynamics*, Vol. 14, No. 3, 1991, pp. 621–628.

[14] Faleiro, L. F., and Pratt, R. W., "Eigenstructure Assignment Applied to the Design of an Autopilot Function for a Civil Aircraft," *Flight Control Systems: Practical Issues in Design and Implementation*, Inst. of Electrical Engineers, Stevenage, England, U.K., 2000, pp. 301–347.

[15] Satoh, A., and Sugimoto, K., "Partial Eigenstructure Assignment Approach for Robust Flight Control," *Journal of Guidance, Control, and Dynamics*, Vol. 27, No. 1, 2004, pp. 145–150.
doi:10.2514/1.9341

[16] Lusardi, J. A., Tischler, M. B., Blanken, C. L., and Labows, S. J., "Empirically Derived Helicopter Response Model and Control System Requirements for Flight in Turbulence," *Journal of the American Helicopter Society*, Vol. 49, No. 3, 2004, pp. 340–349.

[17] Hu, J. S., Yu, S. H., and Hsieh, C. S., "Application of Model-Matching Techniques to Feedforward Active Noise Controller Design," *IEEE Transactions on Control Systems Technology*, Vol. 6, No. 1, 1998, pp. 33–42.
doi:10.1109/87.654875

[18] Heffley, R. K., and Jewell, W. F., "Aircraft Handling Qualities Data," NASA, CR-2144, Washington, D. C., Dec. 1972.

[19] Iwasaki, T., and Skelton, R. E., "All Controllers for the General H_∞ Control Problem: LMI Existence Conditions and State Space Formulas," *Automatica*, Vol. 30, No. 8, 1994, pp. 1307–1317.
doi:10.1016/0005-1098(94)90110-4

[20] Gahinet, P., and Apkarian, P., "A Linear Matrix Inequality Approach to H_∞ Control," *International Journal of Robust and Nonlinear Control*, Vol. 4, No. 4, 1994, pp. 421–448.
doi:10.1002/rnc.4590040403

[21] Ghaoui, L. E., Oustry, F., and AitRami, M., "A Cone Complementarity Linearization Algorithm for Static Output-Feedback and Related Problems," *IEEE Transactions on Automatic Control*, Vol. 42, No. 8, 1997, pp. 1171–1176.
doi:10.1109/9.618250

[22] Zhou, K., Doyle, J., and Glover, K., *Robust and Optimal Control*, Prentice–Hall, Englewood Cliffs, NJ, 1996, pp. 297–300.

[23] SeDuMi, Software Package, Ver. 1.05, McMaster Univ., Hamilton, Ontario, Canada, 2001.

[24] YALMIP, Software Package, Ver. 3, ETH Zurich, Zurich, Switzerland, 2004.

[25] Sato, M., and Satoh, A., "Flight Test of In-Flight Simulator Controller for Simultaneous Simulation of Gust Response and Handling Response," *17th IFAC Symposium on Automatic Control in Aerospace* [CD-ROM], International Federation of Automatic Control, Laxenburg, Austria, 2007.

[26] Sato, M., "Flight Test of Flight Controller for Arbitrary Maneuverability and Wind Gust Rejection," *Proceedings of the Conference on Control Applications*, Inst. of Electrical and Electronics Engineers, Piscataway, NJ, 2006, pp. 2534–2540.